Turkish Journal of Electrical Engineering & Computer Sciences

http://journals.tubitak.gov.tr/elektrik/

Research Article

Turk J Elec Eng & Comp Sci
(2015) 23: 126 – 148

doi:10.3906/elk-1301-182

Enhancing sliding mode control with proportional feedback and feedforward: an experimental investigation on speed sensorless control of PM DC motor drives

Mehmet DAL*
Department of Electricity and Energy, Kocaeli Vocational High School, Kocaeli University, Kocaeli, Turkey

Received: 24.01.2013 • **Accepted:** 19.03.2013 • **Published Online:** 12.01.2015 • **Printed:** 09.02.2015

Abstract: This paper investigates the enhancement of sliding mode control (SMC) with the combined use of feedforward torque compensation and proportional error feedback control. The proposed enhancement is adapted to the control of permanent magnet (PM) DC motor drives by synthesis of the equivalent control equation augmented as proportional feedback and feedforward terms. A novel sliding function, introduced by utilizing the estimated load torque and the estimated rotor current, is examined and compared with another known sliding function obtained by nonideal differentiation of the estimated rotor speed. The significance of the proposed enhancements to SMC consists of the elimination of disturbance, the reduction of the discontinuous control gain magnitude, and the reduction of chattering. The contribution of this study is demonstrated by a performance comparison between several control versions, where the aim is the achievement of good performances in both the speed estimation and state tracking accuracy in the speed sensorless control of PM DC motor drives under varying load inertia. These latter statements are verified by several comparative simulations and experiments.

Key words: Sliding mode control, chattering reduction, sensorless speed control, DC motor drives

1. Introduction

Modern control strategies have prompted the use of the permanent magnet (PM) DC motor as the most efficient and economical actuator for high-performance motion control applications, including guided vehicles, factory automation, robotics, and milling. In these applications, precise position and speed/torque controls are required to perform the required tasks. The bandwidth of the closed loop varies linearly with the load inertia. Therefore, linear controllers, like a fixed-gain proportional plus integral (PI) controller, cannot keep the stability of the closed loop in the case of large inertia variations. However, linear controllers with improved versions are confirmed as the state-of-the-art and most trustable controllers; thus, these controllers have the most widespread applications in industry. Moreover, it has been verified that a combined use of feedforward plus feedback with a linear controller can significantly improve performance in motion control systems, where the feedforward term can eliminate the measurable disturbance effects that arise on the system output [1].

On the other hand, the sliding mode control (SMC) considered in variable structure control is a widely known nonlinear, high-frequency switching feedback control approach. The main advantage of SMC consists of robustness to bounded plant parameter variations and external disturbances, as well, as the fact that SMC has an order reduction property that provides good dynamic response comparable to the behavior of first-order systems [2–4]. In the past decade, therefore, the sliding mode approach has increasingly found a place in the

*Correspondence: mdal@kocaeli.edu.tr

control of electric motor drives and power converters [5–7] and in many other applications, such as automotive and flight controls, robotics, space devices, and the control of chemical process [8]. However, undesired high-frequency oscillations on the system output that are caused by both high-magnitude control gain and nonideal switching action are the main obstacle in the implementation of SMC. This phenomenon, which is known as chattering, can, for example, wear out the mechanical actuators and increase the current ripple in the electrical system. Furthermore, chattering may also lead to instability in closed-loop control systems [9].

Consequently, for the variable structure systems control community, the challenge has arisen to smooth the discontinuous control and reduce the chattering while preserving the main properties of the SMC [10–12]. Reducing the switching control gain directly and/or using a smoothing filter are well-known methods that result in the weakening of the sliding mode and unsatisfactory control performance [13]. A significant number of studies proposed to smooth the discontinuous control were surveyed in [14] and the references therein, where the main concern was to achieve an optimal trade-off between the tracking precision and control bandwidth. However, these solutions are mostly theoretical, and the practical aspect of SMC is not considered much.

This paper aims to combine the advantages of the sliding mode approach with the feedforward torque compensation plus a proportional error feedback to improve the control accuracy and robustness. The proposed combined SMC law is derived by an alternative interpretation of the sliding mode equivalent control equation. The feedforward component combines back-electromotive force (EMF) and the disturbance that arises in the variation of load torque and mechanical parameters. The feedback signal includes the sum of the direct switching SMC plus the proportional error feedback signal. A well-known combined (or integrated) speed control strategy of DC motor drives proposed in [10] is considered as an adequate example to explore the properties of the proposed enhancement to SMC, and its performance is assessed in the operation of a motor drive system under 2 different load inertia. Moreover, a novel switching function, formed using the estimated acceleration, is also examined and compared with another switching function that uses nonideal differentiation of the estimated angular speed. The estimated speed is obtained using a unified sliding mode observer proposed in [10] and the load torque is estimated by the well-known disturbance observer proposed in [15].

The proposed combined SMC has several advantages: rejection of the disturbances that arise in the closed-loop path, considerable reduction of the control gain magnitude, better trajectory tracking in both the transient and steady-state conditions, cancellation of the filtering of the discontinuous control, and the minimization of chattering. These statements are verified by comparative simulations and experiments, which are carried out on a small-sized PM DC motor drive system. The hardware setup uses the recent rapid development of digital signal processor (DSP)-based rapid control prototyping (RCP) tools [16], which make it easy to implement the advanced control strategies without hand code writing.

2. Problem statement

The sliding mode equivalent control is a well-known approach found by recognizing that $\dot{\sigma}(x) = 0$ is the necessary condition to make the state trajectory stay on the sliding surface, $\sigma(x) = 0$ [2]. The SMC design is completed in 2 steps by selecting a constructible switching function $\sigma(x)$ and by synthesizing an adequate control law that can force the system state to reach the sliding surface in a finite time and maintain it there forever. However, the most distinguished ideal features of the SMC can arise when the frequency of the switching control is high, theoretically infinite. However, imperfections in the switching action limits the switching frequency and causes a nonideal sliding motion, where the trajectory remains close to the switching surface $\sigma(x) = 0$. The switching function is the main factor in the formation of the discontinuous control, which naturally changes depending

on the sign of this function. Therefore, the system dynamics under sliding mode are governed by the switching function $\sigma(x)$ and thus by the desired control law, which has to be designed such that the desired dynamics are obtained during sliding mode. A brief presentation of the equivalent control is provided in the following text.

Consider a system defined by $\dot{x} = Ax(t) + B(x)u$; inserting this equation into the differentiation of the switching function $\sigma(x)$ yields:

$$\frac{d\sigma(x)}{dt} = G\dot{x} = GAx(t) + GB(x)u, \tag{1}$$

where the gradient matrix $G = \frac{\partial \sigma}{\partial x}$ corresponds to the slope of the selected sliding surface. In Eq. (1), the control that makes $\dot{\sigma}(x) = 0$ is called the equivalent control, and by replacing u with u_{eq}, it can be calculated from Eq. (1) as:

$$u_{eq} = -\left(GB\right)^{-1} GAx(t), \tag{2}$$

which is not such a control actually applied to the system input, but is rather an interpretation of a control that maintains a sliding motion on the sliding surface $\sigma(x) = 0$ [8]. A conventional direct switching form of SMC is usually given by:

$$u(t) = -Msign(\sigma(t)), \tag{3}$$

where M is the control gain, being a nonzero scalar, and sign is well-known sign function defined as $sign(\sigma(t)) = 1$ for $\sigma(x) > 0$ and $u = \hat{u}_{eq} + Msgn(\sigma_2)$ for $\sigma(x) < 0$.

The exact calculation of the equivalent control as given in Eq. (2) is possible if 2 constraints are satisfied, i.e. the matrix GB has to be invertible, and there must be no disturbance and no parameter variations in the controlled plant. Considering that most real systems have varying parameters, it is assumed that the equivalent control can be captured by passing the discontinuous control in Eq. (3) through a low-pass filter (LPF), i.e. $T\dot{\hat{u}}_{eq}(t) + \hat{u}_{eq}(t) = u(t)$ [2], where $\hat{u}_{eq}$ is the average value or estimation of the ideal continuous control corresponding to the equivalent control given in Eq. (2), and T is the time constant of the LPF used to capture the equivalent control. This approximation can be construed based on the fact that the equivalent control has to be naturally continuous and corresponds to the low-frequency component of the switching control given in Eq. (3). This construing can also be verified as inserting Eq. (2) into Eq. (1) implies the following:

$$\dot{\sigma}(x) = -GB(x)(u - u_{eq}). \tag{4}$$

If the sliding mode exits once, i.e. $\sigma(x) = 0$ and $\dot{\sigma}(x) = 0$, then the equivalent control becomes equal to the actual control u, and the sliding motion will be maintained on the sliding surface $\sigma(x) = 0$. However, with the use of the control in Eq. (3), a high magnitude of control gain is required to push the system state towards the sliding surface and start the desired sliding motion. Unfortunately, not only is the increase of the gain magnitude alone not enough to start a sliding motion, but it also increases the chattering magnitude. As stated previously, reducing the control gain directly or passing the discontinuous control in Eq. (3) through a LPF adversely affects the sliding mode existence. Based on this fact, a fast switching control signal passing through a LPF may exhibit the same behavior as a SMC with a boundary layer using a saturation function [17].

On the other hand, in the case of DC motor drives with an H-bridge converter, a continuous control input is required for pulse-width modulation (PWM) signal generation. Therefore, the control law in Eq. (3) has to be passed through a LPF, but in this case, it provides an unsatisfactory tracking performance in the speed

sensorless control of DC motor drives [18]. This finding necessitates enhancing the SMC law in Eq. (3) in an acceptable manner without losing its main properties.

Many strategies using SMC were proposed in order to improve the control performance and robustness to external disturbances and plant parameter variations for DC motor drives in [19–21] and the references therein. A recent method relevant to the high-order (second-order) SMC approach and proposed for the cascaded control structure of DC motor drives was extensively studied in [22] and the references therein. The disadvantage of this method is the requirement of a high-resolution speed feedback device, which is expensive. In order to reduce the chattering, 2 different gain adaptation techniques proposed in [11] were adapted to current-controlled DC motor drives in [23].

These adaptation techniques, however, were found to be unusable for the combined speed control of DC motor drives in this present study. Consequently, the present paper investigates the further enhancement of SMC with a reasonable assumption, where a combined SMC law is derived by an alternative interpretation of the equivalent control for speed sensorless control of PM DC motor drives.

3. Proposed speed controller

3.1. Plant model

The dynamic model of a PM DC motor can be described by the following well-known equations:

$$\frac{di}{dt} = -\frac{R}{L}i - \frac{k_e}{L}\omega + \frac{1}{L}u, \tag{5a}$$

$$\frac{d\omega}{dt} = -\frac{B}{J}\omega + \frac{1}{J}k_t i - \frac{1}{J}t_L, \tag{5b}$$

where u is the motor supply voltage; i is the rotor current; ω is the rotor angular speed; t_L is the load torque; R and L are the resistance and inductance of the rotor winding, respectively; k_e and k_t are the back-EMF constant and motor torque constant, respectively; B is the viscous friction coefficient, which is usually neglected to simplify the model; and $J(= J_a + J_L)$ is the combined inertia of the rotor and load.

3.2. Switching function

A linear combination between the tracking error of the angular velocity and its derivative is a suitable and usual selection as the switching function for DC servo drive systems.

$$\sigma_1 = c(\omega^* - \omega) + (\dot{\omega}^* - \dot{\omega}) \tag{6}$$

Here, $e_\omega(= \omega^* - \omega)$ and $\dot{e}_\omega(= \dot{\omega}^* - \dot{\omega})$ denote the speed tracking error and its differentiation, respectively. From a theoretical point of view, if the sliding mode exists, i.e. $\sigma_1(t) = 0$ and $\dot{\sigma}_1(t) = 0$, on the switching surface in Eq. (6), then the asymptotic convergence of the state error $(e_\omega(t) = e_\omega(0)e^{-t/c})$ is guaranteed. On the other hand, considering the existence of the sliding mode $c(\omega^* - \omega) + (\dot{\omega}^* - \dot{\omega}) = 0$ implies the rotor current to be:

$$i = \frac{J}{k_t}(c(\omega^* - \omega) + \dot{\omega}^* + \frac{1}{J}t_L), \tag{7}$$

which can be derived by inserting the acceleration in Eq. (5b) into Eq. (6), where the machine parameter B is neglected. This finding verifies that the switching function in Eq. (6) enables one to establish a combined

speed/current control scheme for a DC motor, which is different than the conventional cascaded speed/current control schemes. Moreover, if the existence of sliding mode is guaranteed with the use of Eq. (6), then, at least theoretically, the drive system response becomes dependent on design parameter c only; thus, the controller robustness with respect to parameter variations in the electrical and mechanical subsystem will be improved. In this idea as suggested in [10], however, several practical issues should be considered in the implementation, e.g., the control law in Eq. (3) is unsatisfactory to push the system state towards the sliding surface; thus, an improved control law is required in the implementation [18]. On the other hand, the acceleration signal is required to establish the switching function in Eq. (6), and it is difficult to get it precisely from the direct measurement of the rotor angular speed due to the well-known exact differentiation problem [22]. In digital controlled systems, therefore, the acceleration of the rotor shaft can normally be calculated by nonideal numeric differentiation of the measured angular speed, which can be handled by an incremental encoder, or, alternatively, it can be calculated by a state observer. The angular speed measured by an optical encoder is usually passed through a LPF to suppress the undesired measurement noises, and then a nonideal differentiation can be performed by digital controllers.

In order to improve the control performance of DC motor drives, the modified control version proposed in [18] was given by $u = M\,sign(s_\omega) + G_p e_\omega + k_t\hat{\omega})$, where adding a proportional error feedback term arbitrary to the switching control together with the back-EMF provides better speed tracking performance with respect to both control laws, i.e. the conventional SMC in Eq. (3) and the well-known PI-based cascaded speed/current control. However, with the use of the conventional SMC in Eq. (3), the rotor current ripple is mandatorily acceptable. A further improvement of this control version is proposed in this study, which will be presented in the next section.

3.3. Combined speed controller

A combined speed control strategy, suggested in [10], is considered for a further improved speed sensorless control of DC motor drive in this study. The speed tracking error and its derivative are evaluated as the state variables $\omega^* - \omega \; = e_\omega = x_1$ and $\dot{\omega}^* - \dot{\omega} = \dot{e}_\omega = x_2$, and then a linear combination between the angular speed tracking error and its derivative is defined as the desired switching surface for the drive system.

$$\sigma_1 = cx_1 + x_2 \tag{8}$$

A controllable canonical state space model, which describes the tracking error dynamics in the closed-loop speed control system, is given by:

$$\dot{x}_1 = x_2 = \dot{\omega}^* - \dot{\omega}, \tag{9}$$

$$\dot{x}_2 = \ddot{\omega}^* - \ddot{\omega}, \tag{10}$$

and using Eqs. (5a), (5b), and (7), Eq. (10) is derived as follows:

$$\dot{x}_2 = -\frac{k_t k_e}{JL}cx_1 - \frac{R}{L}x_2 + f(t) - \frac{k_t}{JL}u, \tag{11}$$

where $f(t) = \ddot{\omega}^* + \frac{R}{L}\dot{\omega}^* + \frac{R}{JL}t_L + \frac{k_t k_e}{JL}\omega^* + \frac{k_t}{J}\dot{t}_L$ is imposed as the disturbance entering the closed-loop control path. In [10], the disturbance $f(t)$ is disregarded, expecting that it will be compensated by discontinuous control $u = M\,sign(\sigma)$. However, it is a well-known fact that in real-life systems that operate under SMC, neglected dynamics in the closed loop may result in chattering, which was experimentally verified in [18]. Based on this

finding, a further enhancement to SMC is aimed at in this paper considering an alternative interpretation of Eq. (11). First, inserting Eq. (5a) into Eq. (10) yields

$$\dot{x}_2 = \ddot{\omega}^* - \frac{k_t}{J}\dot{i} + \frac{k_t}{J}\dot{t}_L, \tag{12}$$

and inserting Eq. (5a) into Eq. (12) and then inserting Eq. (7) into the resulting equation gives

$$\dot{x}_2 \ = \ddot{\omega}^* - \frac{k_t R}{JL}\underbrace{\frac{J}{k_t}\left(c(\omega^* - \omega) + \dot{\omega}^* + \frac{1}{J}t_L\right)}_{i} + \frac{k_t k_e}{JL}\omega - \frac{k_t}{JL}u + \frac{k_t}{J}\dot{t}_L. \tag{13}$$

Eq. (13) can then be rewritten as

$$\dot{x}_2 = \frac{R}{L}cx_1 - \frac{k_t}{JL}u + f_m(t), \tag{14}$$

with $f_m(t) = \ddot{\omega}^* + \frac{R}{L}\dot{\omega}^* + \frac{R}{JL}t_L + \frac{k_t}{J}\dot{t}_L + \frac{k_t k_e}{JL}\omega$. Now, considering the definition of the equivalent control, it can be derived by taking the time derivative of Eq. (8) and then equating it to 0.

$$\dot{\sigma}_1|_{u=u_{eq}} = c\dot{x}_1 + \dot{x}_2 = 0 \tag{15}$$

Inserting both Eqs. (9) and (14) into Eq. (15) gives the following:

$$\dot{\sigma}_1 = \ c\dot{x}_1 + \frac{R}{L}cx_1 - \frac{k_t}{JL}u + f_m(t). \tag{16}$$

Supposing that the sliding mode $\sigma_1(t) = 0$ is achieved imposes a validity of constraint $\dot{x}_1 = -cx_1$ that can be derived from Eqs. (8) and (9), and then, equating Eq. (16) as 0 and solving it for u_{eq} $(= u)$ gives:

$$u_{eq} = \frac{JL}{k_t}(\frac{R}{L} - c)cx_1 + \frac{JL}{k_t}f_m(t), \tag{17}$$

where u_{eq} is the exact equivalent control, which is difficult to calculate as given in Eq. (17) due to imperfect knowledge of the system parameters. Therefore, equivalent control in Eq. (17) can be modified as:

$$\hat{u}_{eq} = \underbrace{G_p(\omega^* - \omega)}_{u_{fb}} + \underbrace{\hat{d}(t) + k_e\omega}_{u_{ff}}, \tag{18}$$

where the first term, $G_p(\omega^* - \omega)$, can be interpreted as a proportional error feedback denoted by u_{fb} with the gain constant $G_p = \frac{JL}{k_t}(\frac{R}{L} - c)\,c$, and the last term can be considered as the feedforward control, u_{ff}, which is interpreted as the sum of the disturbance and back-EMF, i.e. $u_{ff} = \hat{d}(t) + k_e\omega$, where the disturbance that arises in the closed-loop path is given by $\hat{d}(t) = \frac{JL}{k_t}(\ddot{\omega}^* + \frac{R}{L}\dot{\omega}^* + \frac{R}{JL}\hat{t}_L + \frac{k_t}{L}\dot{\hat{t}}_L)$. In Eq. (18), $\hat{u}_{eq}$ denotes the best estimate of the exact equivalent control given in Eq. (17), where the load torque t_L is normally unknown in most cases. Thus, in Eq. (18), the estimated load torque $\hat{t}_L$ and its derivative are used instead of their real values. However, variation of the motor parameters is disregarded in this study. The estimated load torque is obtained using a disturbance observer proposed in [15]. A brief structural explanation of this observer will be given in a further section.

As stated above, the representation of the equivalent control as given in Eq. (18) leads to finding a novel combined control law. The equivalent control in Eq. (18) is a continuous control signal corresponding to the average value of the discontinuous control in Eq. (3) when a sliding motion exists on the sliding surface $\sigma_1(t) = 0$. However, the existence of the sliding mode $\sigma_1(t) = 0$ is not guaranteed. Hence, a desired control can be obtained by the Lyapunov approach to attempt to ensure that the state trajectory reaches the sliding surface in a finite time and remains there forever. To this end, inserting Eq. (18) into Eq. (16) yields the following:

$$\dot{\sigma}_1 = \frac{k_t}{JL}(\hat{u}_{eq} - u), \tag{19}$$

where it can be easily seen that the equivalent control converges to the desired control ($u_{eq} \to u$) if the sliding mode exits, $\sigma_1 \to 0$ and $\dot{\sigma}_1 \to 0$. According to the Lyapunov stability criteria, this can be ensured by satisfying the reaching condition $\sigma_1\dot{\sigma}_1 < 0$, which imposes $\dot{\sigma}_1 = -Nsgn(\sigma_1)$, where N is a positive scalar constant selected by a designer. Now, solving Eq. (19) for u yields a novel control law denoted as u_1:

$$u_1 = \hat{u}_{eq} + \eta sgn(\sigma_1), \tag{20}$$

with $\eta = N\frac{JL}{k_t}$. Moreover, in this study, a modified version of the sliding variable is also proposed. This can be derived by inserting the acceleration in Eq. (5b) into Eq. (6):

$$\sigma_2 = c(\omega^* - \omega) + (\dot{\omega}^* - \frac{k_t}{J}\hat{i} + \frac{1}{J}\hat{t}_L). \tag{21}$$

One significant advantage of using this switching function is that it cancels out the requirement of the differentiation of the angular speed to get the acceleration signal, which is normally problematic, especially when the speed trajectory includes some sudden sharp changes. Moreover, the estimated acceleration used in Eq. (21) acts as active inertia providing higher stiffness. Therefore, the reflection of the load torque in the feedback path can compensate for the disturbances caused by variation of the load, which can generate unacceptable motion errors. Consequently, considering the novel sliding function in Eq. (21) implies the modified control version to be:

$$u_2 = \hat{u}_{eq} + \eta sgn(\sigma_2). \tag{22}$$

It should be noted that in the case of speed sensorless control implementation, the measured angular speed ω used in Eqs. (21) and (22), as well as in the feedback loop, has to be replaced by its estimate $\hat{\omega}$.

The control law in Eq. (22) is represented by a signal flow diagram in Figure 1, where only the establishment of the sliding function σ_2 is considered. Choosing small values for the control gains $\eta$and G_p reduces the chattering and cancels out the requirement for a LPF, which is generally needed for smoothing the discontinuous control switched with a high magnitude gain. Considering that the disturbance arising in the closed-loop path can be obtained by estimation, adding the estimated disturbance as a feedforward term together with a proportional error feedback to the switching control can improve the tracking accuracy and the robustness in respect to the variation of load torque.

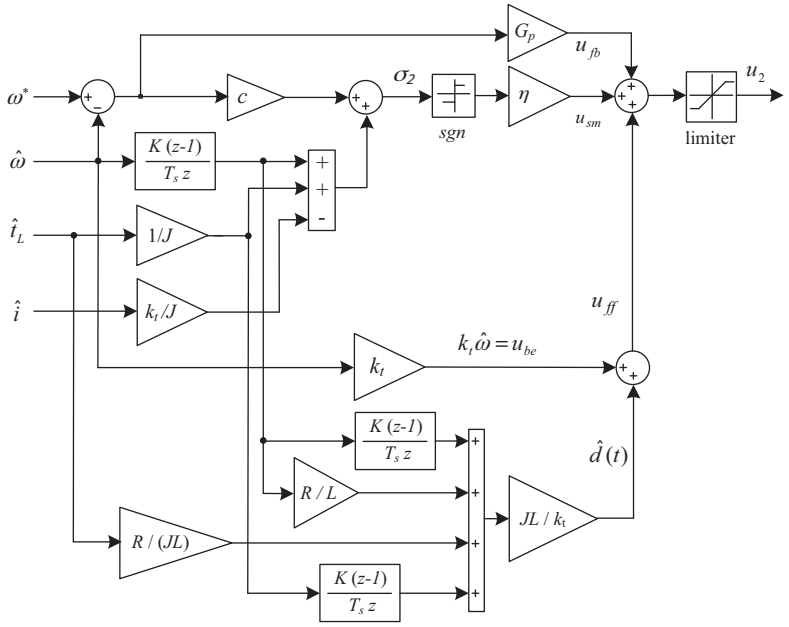

Figure 1. Signal flow diagram of the proposed sensorless controller given in Eq. (22).

4. Observers

4.1. Sliding mode speed and current observer

In the case of DC motor drives, the unified sliding mode observer proposed in [10] is used in order to estimate both the rotor current and the angular speed. This observer's structure is briefly explained by considering its model, given as follows:

$$\frac{d\hat{i}}{dt} = -\frac{R}{L}\hat{i} + \frac{1}{L}u - \frac{L_1}{L}sgn(e_i), \tag{23}$$

where $\hat{i}$ is the estimated rotor current, $e_i = \hat{i} - i$ is the current estimation error, and $L_1 sgn(e_i)$ is a nonlinear term that is replaced with the back-EMF $(k_e \times \omega)$ in Eq. (5a) and corresponds to the observer's discontinuous control. $L_1 > 0$ is the observer control gain constant that serves a similar purpose, as in the well-known Luenberger observer. The observer in Eq. (22) requires the rotor measured current i and the control input u, which corresponds to the motor terminal voltage. In the implementation, the terminal voltage u is not easy to handle by measurement due to the presence of PWM modulated signals at the motor terminals. Thus, it is usually replaced by the control input in Eq. (20) or (22). A control input is also used as the reference voltage vector required for the PWM signal generation. Moreover, the observer's control input, $L_1 sgn(e_i)$, has to be passed through a LPF to extract the estimated speed denoted by $\hat{\omega}$.

In general, the effectiveness of an observer is assessed by examining the estimation error dynamics, which can be obtained by subtracting Eq. (5a) from Eq. (23):

$$\frac{de_i}{dt} = -\frac{R}{L}e_i + \frac{k_e}{L}\omega - \frac{L_1}{L}sgn(e_i), \tag{24}$$

where the control input u_1 or u_2 is assumed to converge to the desired supply voltage applied to the rotor winding; thus, whenever the reaching condition $e_i\dot{e}_i < 0$ occurs, a sliding motion starts on the sliding surface,

$e_i = 0$. To this end, gain L_1 must be selected to satisfy the inequality $|k_e\omega| < L_1$, which implies the decaying of the current estimation error and its derivative to 0, i.e. $e_i \to 0$ and $\dot{e}_i \to 0$, in a finite time. The value of L_1 can be determined by a trial-and-error method in simulation.

The rotor angular speed can be extracted from Eq. (24) by averaging the discontinuous control of the observer, i.e. passing term $L_1 sgn(e_i)$ through a LPF and then dividing it into machine constant $k_e(= k_t)$, i.e.:

$$\hat{\omega} = \frac{(L_1 sgn(e_i))_{eq}}{k_t}, \tag{25}$$

where $(L_1 sgn(e_i))_{eq}$ corresponds to the average value of the discontinuous observer's discontinuous control $L_1 sgn(e_i)$. A tunable digital first-order LPF is used for averaging the observer control, and the details regarding the implementation of this observer can be found in [18].

4.2. Disturbance observer

The disturbance observer devoted to estimating the load torque is required for both purposes, i.e. to compensate for the disturbance that arises at the control loop and to establish the proposed sliding function σ_2. The load torque is estimated using a well-known disturbance observer [15], which can be structured in accordance with Eq. (5b):

$$t_L = k_t i - J\frac{d\omega}{dt}, \tag{26}$$

where parameter B is neglected again. It is also assumed that the disturbance arises from the variations of the load torque and the mechanical parameters. The differentiation task is usually performed using a first-order LPF. Thus, in order to calculate the disturbance torque, the measured current and angular speed of the rotor are processed in the model in Eq. (27). In the case of sensorless drives, the angular speed ω is replaced with its estimate $\hat{\omega}$. The replacement of the differentiation task with a LPF forces the basic structure of the disturbance observer to be

$$\hat{t}_L = \frac{g}{s+g}(k_e i - Js\hat{\omega}) = \frac{g}{s+g}(gJ\hat{\omega} + k_e i) - gJ\hat{\omega}, \tag{27}$$

where $\hat{t}_L$ denotes the estimated disturbance torque and g is the corner frequency of the LPF. Issues regarding different implementations of this observer can be found in [21].

4.3. Stability analysis

The stability of the overall system is hard to prove when the observers' models are taken into account; however, it can be verified by means of Lyapunov assumption that all of the estimated variables, such as the rotor speed, the rotor current, and the load torque, converge to their real values, as well as neglecting variation of the parameters. Based on this assumption, for example, considering the control law in Eq. (22), a Lyapunov-based stability analysis can be verified by satisfying the reaching condition $\sigma_2\dot{\sigma}_2 < 0$ that imposes $\dot{\sigma}_2 = -\lambda sgn(\sigma_2)$. Now multiplying both sides of $\dot{\sigma}_2 = -\lambda sgn(\sigma_2)$ by σ_2 yields

$$\sigma_2\dot{\sigma}_2 < -\lambda\,|\sigma_2|\,. \tag{28}$$

Inserting Eq. (21) into Eq. (28) and then inserting Eq. (22) into the resulting equation gives:

$$\sigma_2\frac{k_t}{JL}(u_{eq} - \hat{u}_{eq}) - \frac{k_t}{JL}\eta\,|\sigma_2| < -\lambda\,|\sigma_2|\,, \tag{29}$$

where $\hat{u}_{eq}$ is assumed as the best estimate of the actual equivalent control u_{eq}. The estimation error, therefore, is assumed to be bounded by some known function $F(x_1, \dot{x}_1, \ddot{x}_1) = F$, i.e. $|u_{eq} - \hat{u}_{eq}| < F$, so selecting $\frac{k_t}{JL}\eta = (F + \lambda)$ implies

$$\sigma_2(u_{eq} - \hat{u}_{eq}) - F\,|\sigma_2| - \lambda\,|\sigma_2| < -\lambda\,|\sigma_2|\,, \tag{30}$$

which satisfies the desired stability condition.

5. Simulations

In this section, several comparative simulations are performed in order to explore the properties of the proposed control laws, u_1 and u_2. In the simulations, the sliding functions in Eqs. (6) and (24) have to be modified for speed sensorless drives by replacing the measured angular speed ω with its estimate $\hat{\omega}$. Next, modified versions of the sliding functions take the following forms, respectively:

$$\sigma_1 = c(\omega * -\hat{\omega}) + c(\dot{\omega} * -\dot{\hat{\omega}}), \tag{31}$$

$$\sigma_2 = c(\omega^* - \hat{\omega}) + (\dot{\omega}^* - \frac{k_t}{J}\hat{i} + \frac{1}{J}\hat{t}_L), \tag{32}$$

where the estimated angular speed and its nonideal differentiation are directly utilized in Eq. (31) to establish sliding variable σ_1, but the rotor current or its estimate $\hat{i}$ and estimated load torque $\hat{t}_L$ are used in Eq. (32) to establish variable σ_2. Consequently, these modifications force the proposed control versions u_1 and u_2 to be modified as follows:

$$u_1 = \hat{u}_{eq} + \lambda sgn(\sigma_1), \tag{33}$$

$$u_2 = \hat{u}_{eq} + \lambda sgn(\sigma_2), \tag{34}$$

where the estimated equivalent control is given by $\hat{u}_{eq} = G_p(\omega^* - \hat{\omega}) + \hat{d}(t) + k_e\hat{\omega}$. The modified control versions in Eqs. (33) and (34) are examined with regards to important issues such as chattering reduction, speed tracking accuracy, and estimation convergence. Moreover, performance comparisons are performed between the proposed control u_2 and an improved PI-based speed/current control, and between u_2 and a conventional SMC that has a high magnitude gain and also uses a LPF.

Using Simulink blocks, a flexible speed sensorless control scheme of the DC motor drive system is built, similar to the hardware system configuration described in a later section. However, the H-bridge power converter and the PWM modulator are assumed to be ideal so their models are not given in the simulation scheme. A time sampling of 200 μs is used, and the same operation conditions are considered for all of the control versions. For example, the motor is operated imposing a reversal square-wave speed command with $\omega^* = \pm 200$ rad/s under the same constant load torque. An on-line transition between the control versions can be achieved by activating software switches inserted into the control scheme. The machine name plates and parameters are listed in the Table below.

Test 1: In order to explore the properties of sliding functions σ_1 and σ_2, these functions are examined first by a conventional SMC, $u = Msgn(\sigma)$ with a smoothing filter and a high magnitude gain M (=12). The corner frequency of the LPF used in the torque observer is determined as 80 rad/s by the trial-and-error method. The obtained results are shown comparatively in Figure 2a, where the speed tracking performance fails, and a high magnitude of chattering (oscillation) arises on the rotor current when σ_1 is used (between 0 and 1 s). In contrast, a significant improvement in the speed tracking performance is achieved when σ_2 is used (between

0 and 2 s), and the chattering magnitude appearing on the rotor current is reduced, as well. Moreover, the disturbance observer is also examined; for example, the convergence of the torque estimation, i.e. $\hat{t}_L \rightarrow t_L$, and a graph of the sliding function variables σ_1 and σ_2 are plotted in Figure 2b, respectively. It is easily seen that the proposed sliding function, σ_2, is much smoother and has a lower magnitude with respect to σ_1. This might be the reason why each controller provides a different response.

Table. Name plates and motor parameters.

Quantity	Symbol	Unit
Nominal voltage	V_{dc}	12 V
No-load speed	n	580 rad/s
Max. continuous current	i_m	1.5 A
Max. continuous torque	t_{em}	28.4e-3 Nm
Back-EMF constant	k_e	0.0195 Vs/rad
Torque constant	k_t	0.0195 Nm/A
Rotor resistance	R	2.5 Ω
Rotor inductance	L	0.3 mH
Inertia of motor	J	17.2e-7 kg m^2
Inertia of flywheel	J_1	14.2e-6 kg m^2
Inertia of flywheel	J_2	30.2e-6 kg m^2
Viscous damping constant	B	1e-6 Nms/rad

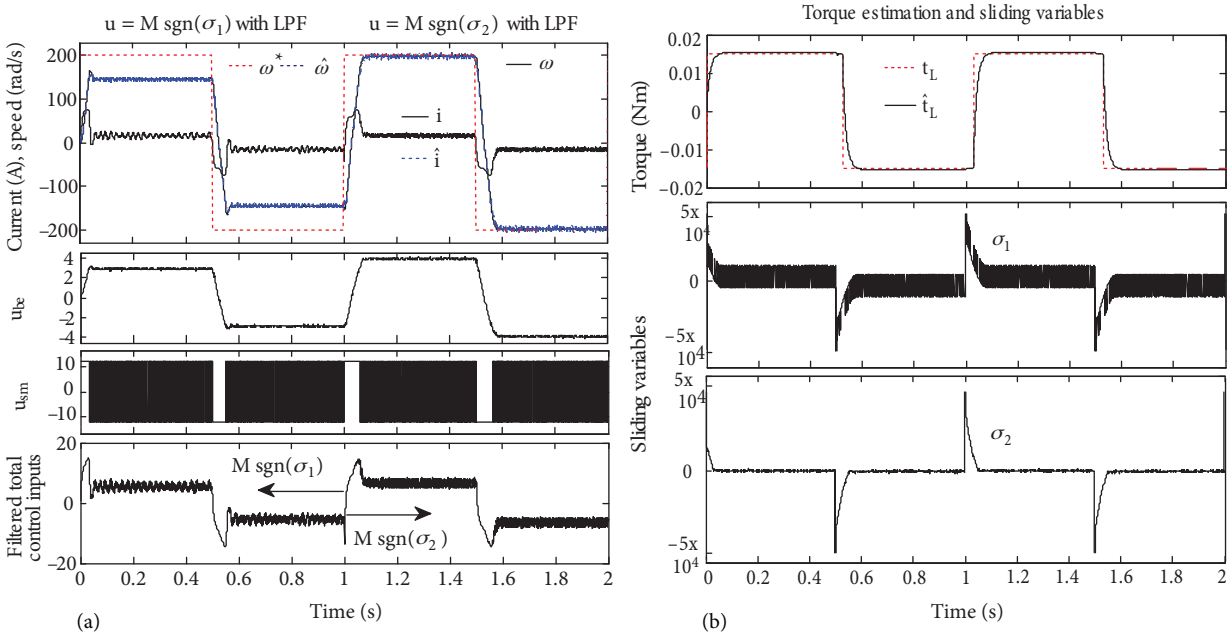

Figure 2. a) Response of conventional SMCs $Msgn(\sigma_1)$ and $Msgn(\sigma_2)$ (top), control components (middle), and filtered total control input (bottom); b) convergence of the estimated disturbance torque to the load torque (top) and sliding variables σ_1 and σ_2 (middle and bottom, respectively).

Test 2: The proposed control versions, u_1 in Eq. (33) and u_2 in Eq. (34), are examined comparatively without requiring a LPF for the same tuning parameters of $c = 100$, $\eta = 0.4$, and $G_p = 0.2$, which are determined by trial-and-error method. The observer control gain in Eq. (23) is selected as $L_1 = 10$, and the corner frequency

of the LPF used in this observer is chosen as 75 rad/s. A comparative result is plotted in Figure 3a, where u_1 is activated for the first half of the simulation time (between 0 and 1 s) and control version u_2 takes place in the second half of the simulation time (between 1 and 2 s). The components of each control version are plotted separately in Figure 3b. These components, respectively, are the back-EMF denoted by u_{be}; the estimated disturbance $\hat{d}(t)$; the discontinuous controls $\lambda sgn(\sigma_1)$ and $\lambda sgn(\sigma_2)$, both of which are denoted by u_{sm}; and the proportional error feedback denoted by u_{fb}, whose significance arises at the transients.

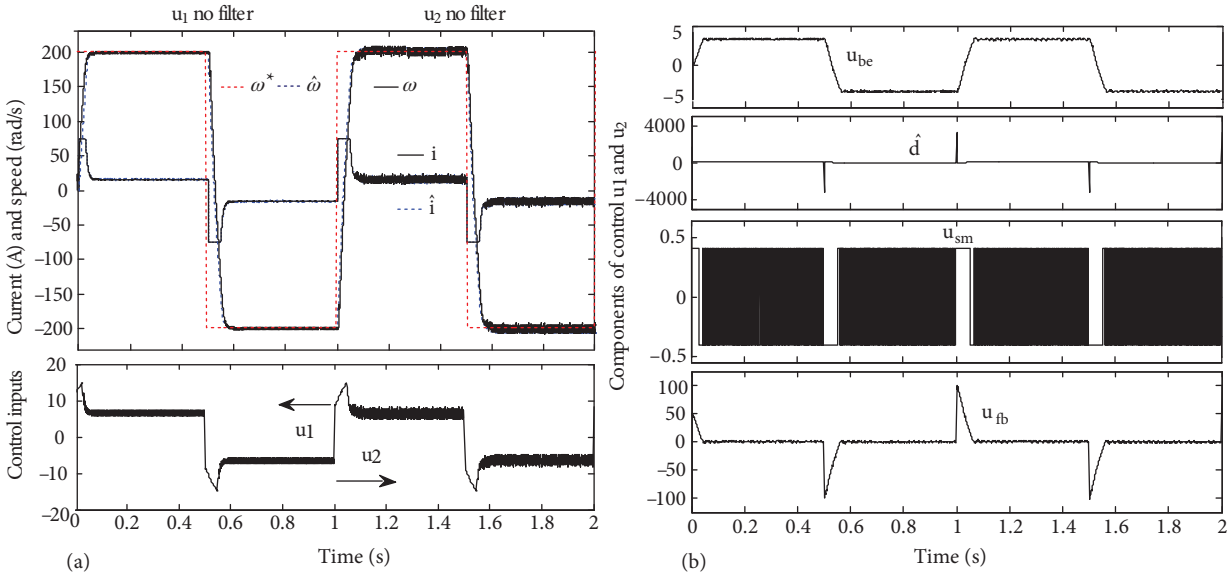

Figure 3. Response of the control versions: a) u_1 and u_2 (top), control inputs u_1 and u_2 (bottom); b) components of control u_1 (between 0 and 1 s) and u_2 (between 1 and 2 s).

In the next simulation, Test 2 is repeated in order to explore how the performances of both control versions, u_1 and u_2, are affected when the disturbance $\hat{d}(t)$ is not injected. The obtained results are plotted in Figure 4, where an unsatisfactory performance is obtained in the tracking and estimation of the speed with respect to the previous test result shown in Figure 3, where injecting $\hat{d}(t)$ into each controller improves the trajectory tracking performance. Moreover, without injecting $\hat{d}(t)$, the response of control u_1 is adversely affected more than that of control u_2. This can be observed clearly in Figure 4.

The next simulation is performed for a performance comparison between the proposed control version u_2 and the improved cascade PI current/speed control proposed in [21]. The relevant results are plotted in Figure 5, where tracking of the rotor speed and current (top) and control signals u_{PI} and u_2 (bottom) are shown in the left column and the magnified responses are shown in the right column. The superiority of the proposed controller u_2 with respect to the improved u_{PI} controller arises with a faster response time, a better suppression in current ripple, and no overshoot, which can be observed in the right column in Figure 5. These comparative results also verify the fact that with proper selection of the sliding function, the performance of the SMC can be improved.

In addition, several simulations are performed in order to explore the distinction between the controllers' robustness and the variation of the speed. Therefore, all 3 control versions mentioned above are examined for various speed ranges. First, the speed tracking performances of the controllers are examined under a constant

load (0.02 Nm) operation mode for a low range of reversal speed with 30 rad/s, and the obtained results are plotted in Figure 6. Comparing the results in Figures 6a and 6b verifies that both proposed control versions, u_1 and u_2, provide lower speed ripple and lower current ripple with respect to improved u_{PI} control. However, at this low range of speed, the improved u_{PI} control exhibits a faster transient response.

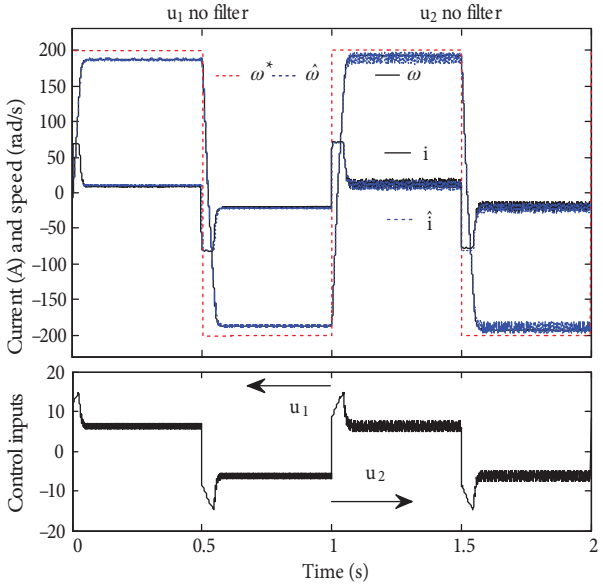

Figure 4. The response of control versions u_1 and u_2 without the injection of the $\hat{d}(t)$ (top), control inputs (bottom).

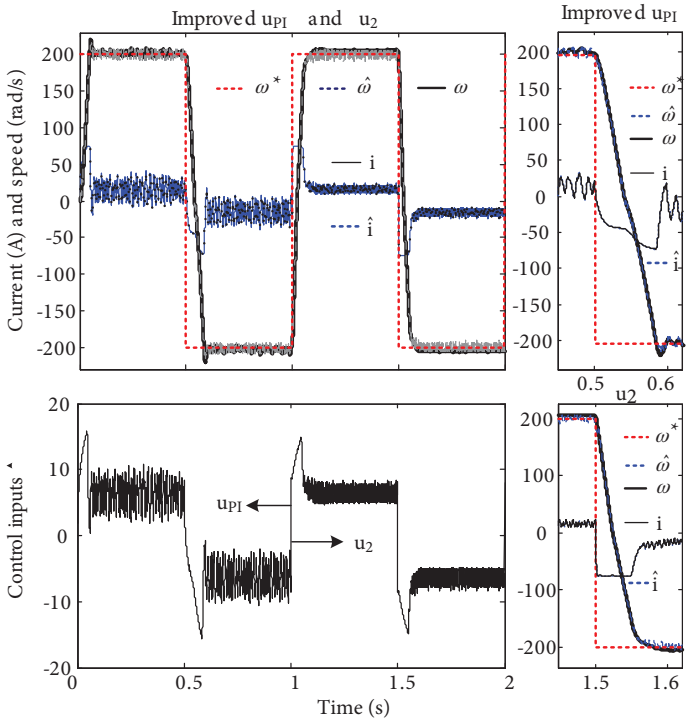

Figure 5. Reponses of the control u_2 and improved u_{PI}: tracking of the rotor speed and current (top) and control inputs (bottom) in the left column, and magnified responses of u_{PI} and u_2 in the right column.

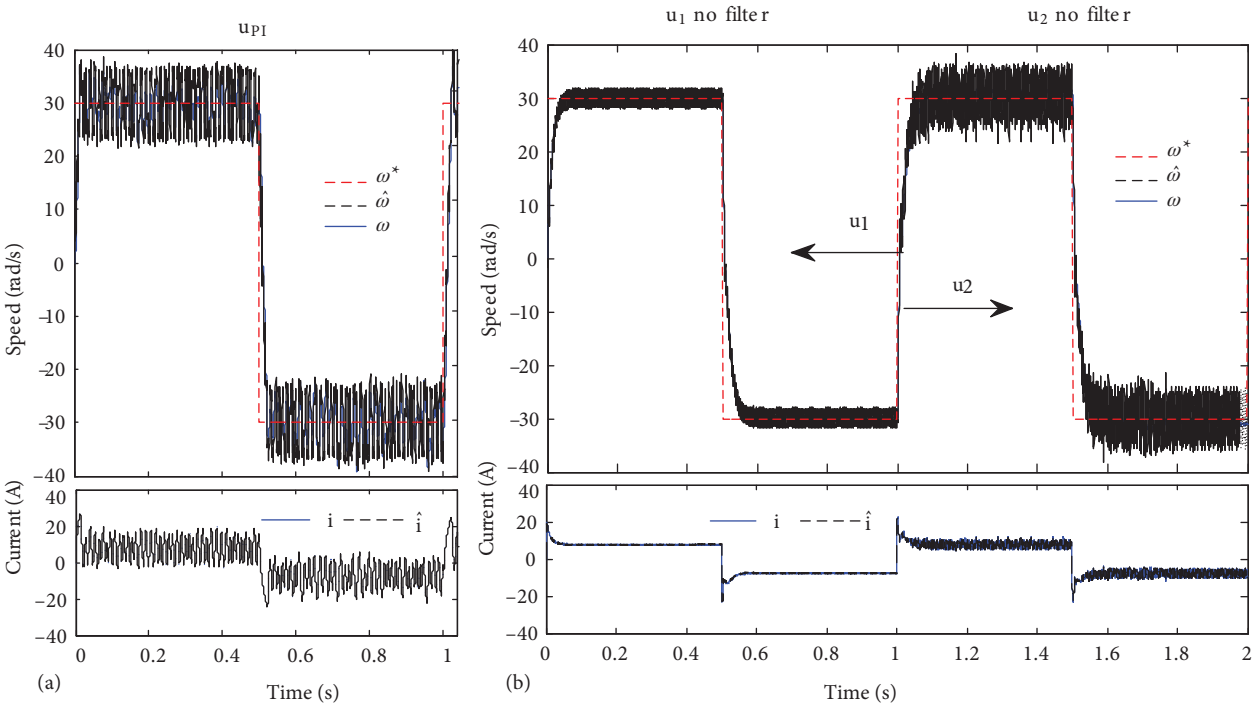

Figure 6. Reponses of the controllers for a lower range reversal speed with 30 rad/s: **a)** for improved u_{PI}, **b)** for both u_1 and u_2.

Moreover, the speed tracking performance is also examined under a constant load (0.02 Nm) operation mode with varying stepped speed ranges (starting at 0 and increasing step-by-step to 50 rad/s, 100 rad/s, and 300 rad/s). The relevant results with an enlargement of the transients' responses are plotted in Figure 7. As mentioned above, in a sensorless drive, the improved u_{PI} control version provides larger ripples and larger overshoot in the current and speed with respect to the proposed control versions u_1 and u_2. This can be seen from comparing Figures 7a, 7b, and 7c, where the transient speed response time seems to be the same for all of the control versions. For the later simulations, the current traces, i.e. i and $\hat{i}$ in Figures 6 and 7, are magnified at a multiplication of 10 for better observation.

6. Hardware setup and experiments

6.1. Hardware setup

The experimental setup, called the DSP-2 DC experimental system, is shown in Figure 8. It consists of several hardware and software components [16]. These are a small-sized PM DC (ESCAP) motor (with a low-resolution encoder), a transistorized H-bridge power converter with a current and a voltage sensor, and a digital control board called DSP-2. The DSP-2 controller, based on the TI TMS320C32-60 core and FPGA Xilinx CS40-PQ240, can communicate with host PCs via a USB port with a serial RS-232 converter and has its own RCP tools based on MATLAB/Simulink and the Real-Time Workshop toolbox. Thus, the control algorithms can be easily programmed using the Simulink building blocks, and after the build-in process, the generated codes are executed in real time within the DSP-2 controller. In all of the experiments, a sampling period of 200 μs is used to execute the control algorithm. The software 'Terminal' running on the host PC provides a graphical user interface for data visualization and parameter tuning while the system operates.

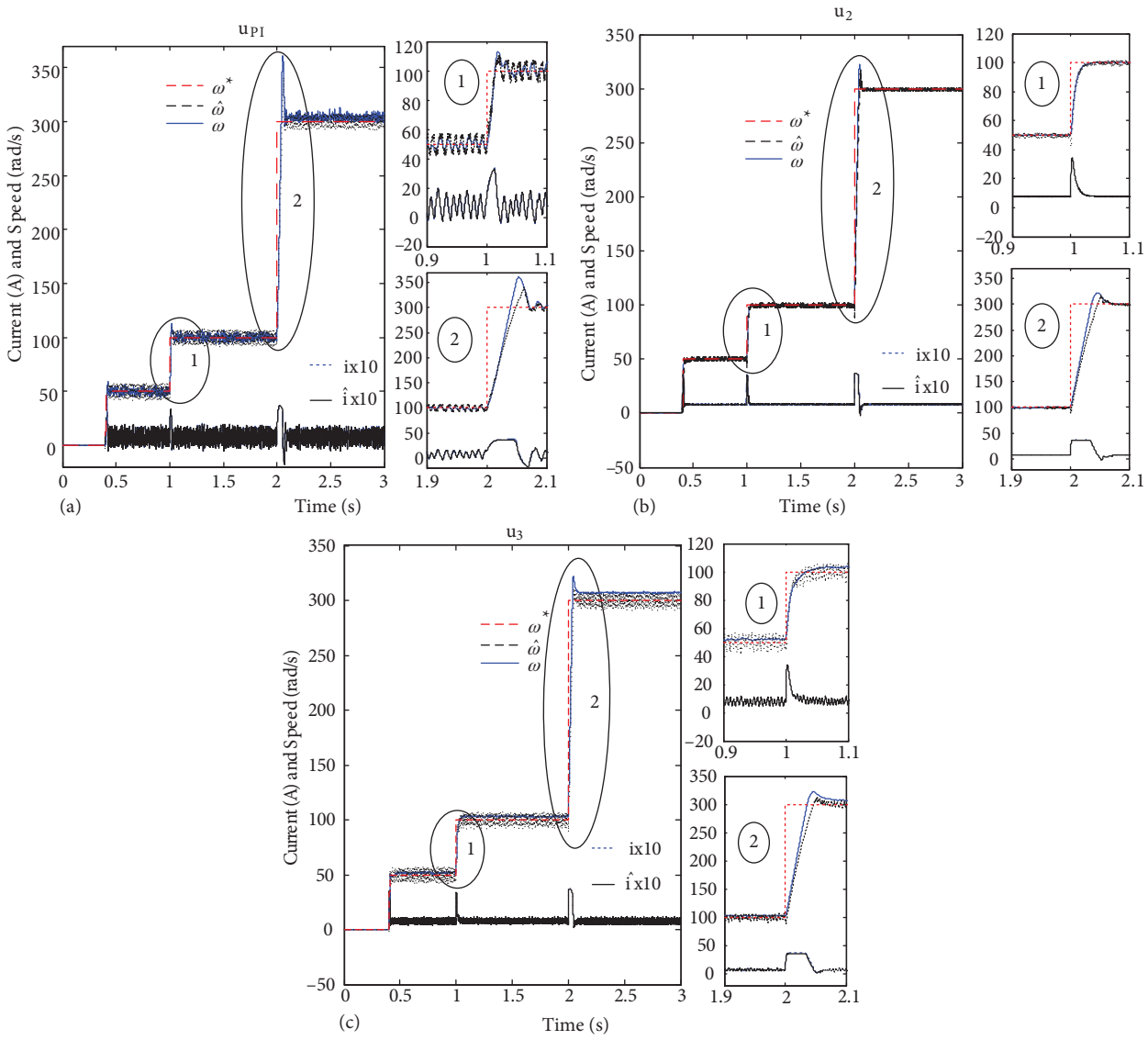

Figure 7. Reponses of the controllers for stepped speed ranges for: a) the improved u_{PI}, b) control version u_1, c) u_2.

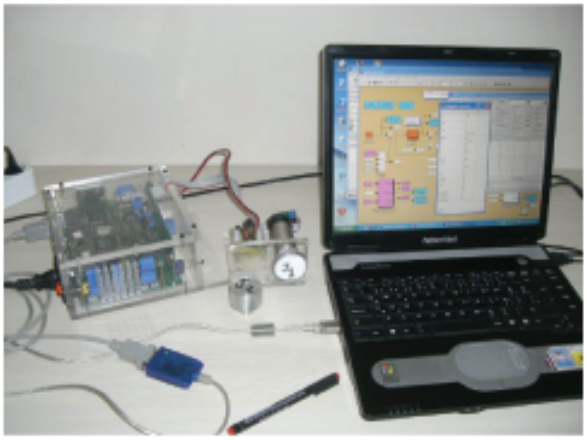

Figure 8. DSP-2-based DC experimental system.

In order to load the motor, 2 differently sized aluminum flywheels, a small one with inertia J_1 and a large one with J_2, are used. The load variation is performed by exchanging these apparatuses consecutively, i.e. each flywheel is mounted on the rotor shaft manually when the relevant study is required.

The overall configuration of the proposed control scheme is illustrated in Figure 9, where all of the requisite control algorithms in the relevant blocks are programmed using MATLAB/Simulink, and executed by the DSP-2 controller after the build-in process. In the control scheme, several software switches are employed in order to perform an easy transition without repeating the build-in process, e.g., s_{w1} enables altering the speed feedback signal between the estimated or measured one. Similarly, s_{w2} can alter control versions to activate consecutively. Hence, sensored and sensorless drives using the proposed control versions can be used optionally, making 1 or 0 the value on the pane of the parameter dialogue box shown on the DSP-2 terminal screen in Figure 8.

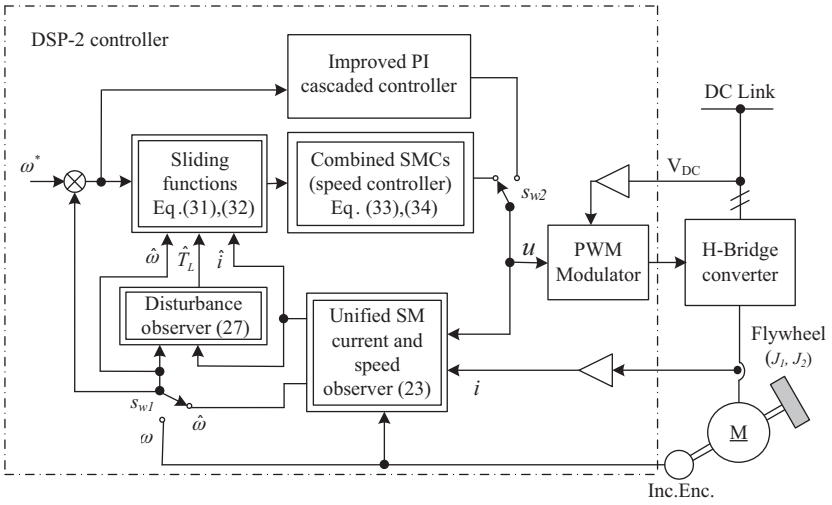

Figure 9. Overall configuration of the proposed control scheme.

6.2. Experimental results

The performance of the sensored and sensorless SMC having a high magnitude gain was compared with the conventional PI speed/current controller in [18]. Therefore, in this section, several comparative experiments carried out on the DSP-2 experimental setup are presented in order to explore the distinction between the proposed control laws and the others mentioned above. In all of the experiments, the design parameters, i.e. $c = 100$, $\eta = 0.5$, and $G_p = 0.5$, determined by trial-and-error method are used.

Experiment 1: The first comparison is considered between the hybrid control version proposed in [18] and the modified SMC version u_1. The second comparison is considered between the improved PI controller proposed in [21] and the novel proposed control u_2. These tests are carried out while a light load (flywheel with J_1) acts on the rotor shaft and a reversal square-wave reference speed $\omega^* = 200$ rad/s is used. The response of the high gain version SMC in [18] and u_1 is plotted in Figure 10a; similarly, the response of the improved u_{PI} and u_2 is plotted in Figure 10b. In this test, u_1 and u_2 are examined without injecting estimated disturbance $\hat{d}(t)$. In this case, the obtained results verify that all of the control versions, u_1, u_2, and u_{PI}, exhibit almost the same performance in terms of speed tracking accuracy while the light load acts on the rotor shaft. However, as can be seen in Figure 10a, proposed control laws u_1 and u_2 significantly reduce the magnitude of the current ripple (or chattering) in respect to the significantly reduced chattering that arises on the rotor current in respect

to the control law proposed in [18], where a high gain ($M = 12$) and proportional error feedback were used. It should be noted that in cascaded PI-based control schemes, the response time of the speed controller is determined by the reference current, which is normally limited to 1.5 times the nominal load current of the relevant motor. This is normally achieved by a limiter that is placed at the output of the speed controller. However, the combined SMC scheme has a single-loop control structure and the unlikely cascaded structure of the PI-based speed/current control scheme. Therefore, there is no mechanism that can limit the rotor current reference; thus, inherently, it can reach a value of twice its nominal value depending on the acceleration of the rotor shaft. Based on this, in the improved PI-controlled drive scheme, the reference current is limited intentionally by twice its nominal value to make sure that the operation constraints are the same for all of the compared control versions.

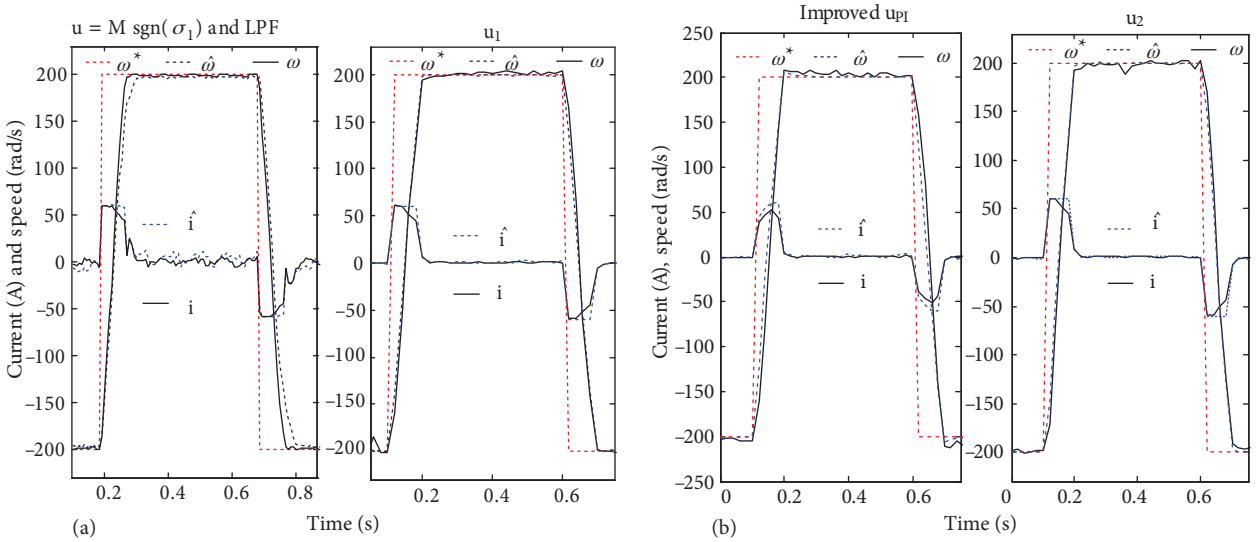

Figure 10. Responses of the control versions for load inertia J_1: a) response of the SMC with the LPF and a high-magnitude gain, and of control u_1; b) response of u_2 and the improved u_{PI}.

Experiment 2: In order to explore the robustness of the proposed control laws with respect to the load variation, experiment 1 is repeated for the flywheel with inertia J_2, which has a larger value with respect to J_1. In this case, the obtained results regarding the rotor electromagnetic torque $t_e\,(= k_t xi)$ and estimated load torque $\hat{t}_L$ are shown in Figure 11a, where the graphics reflect the typical characteristics of the flywheel acting on the rotor shaft. The variation of sliding variables σ_1 and σ_2 with respect to time are also plotted in Figure 11b, which verifies that σ_2 has a smoother and lower magnitude waveform than that of σ_1, which is also verified in the simulation.

Performance comparisons between the improved PI control u_{PI} and the proposed control versions (u_1 and u_2) are also performed. The responses of the controllers to the current and speed trajectories are shown in Figure 12, where each control input and associated components are given in the left column. Control versions u_1 and u_2, are examined without injecting the disturbance $\hat{d}(t)$, and the obtained result is plotted in Figures 12a and 12b, respectively. The response of the improved u_{PI} control version is shown in Figure 12c. All 3 controllers, u_{PI}, u_1, and u_2, provide almost the same performance in the tracking of the speed and the current. Concerning these results, it can be noted that the feedback component u_{fb} suppresses the speed tracking error at the transient instant for control versions u_1 and u_2, and component u_{be} compensates for the back-EMF effect depending on the angular speed variations for all of the control versions.

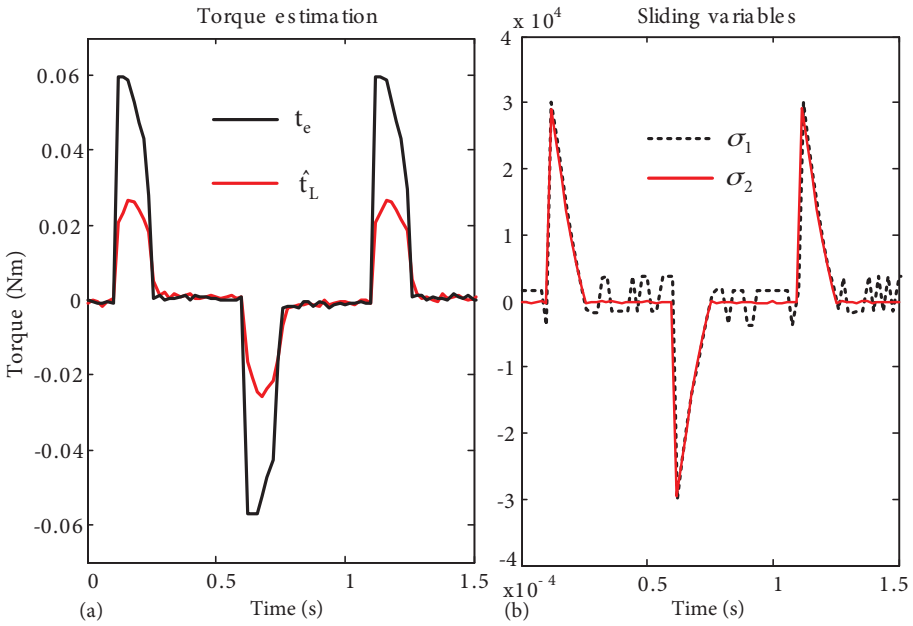

Figure 11. a) Calculated electromagnetic torque t_e and estimated load torque $\hat{t}_L$, b) sliding variables σ_1 and σ_2.

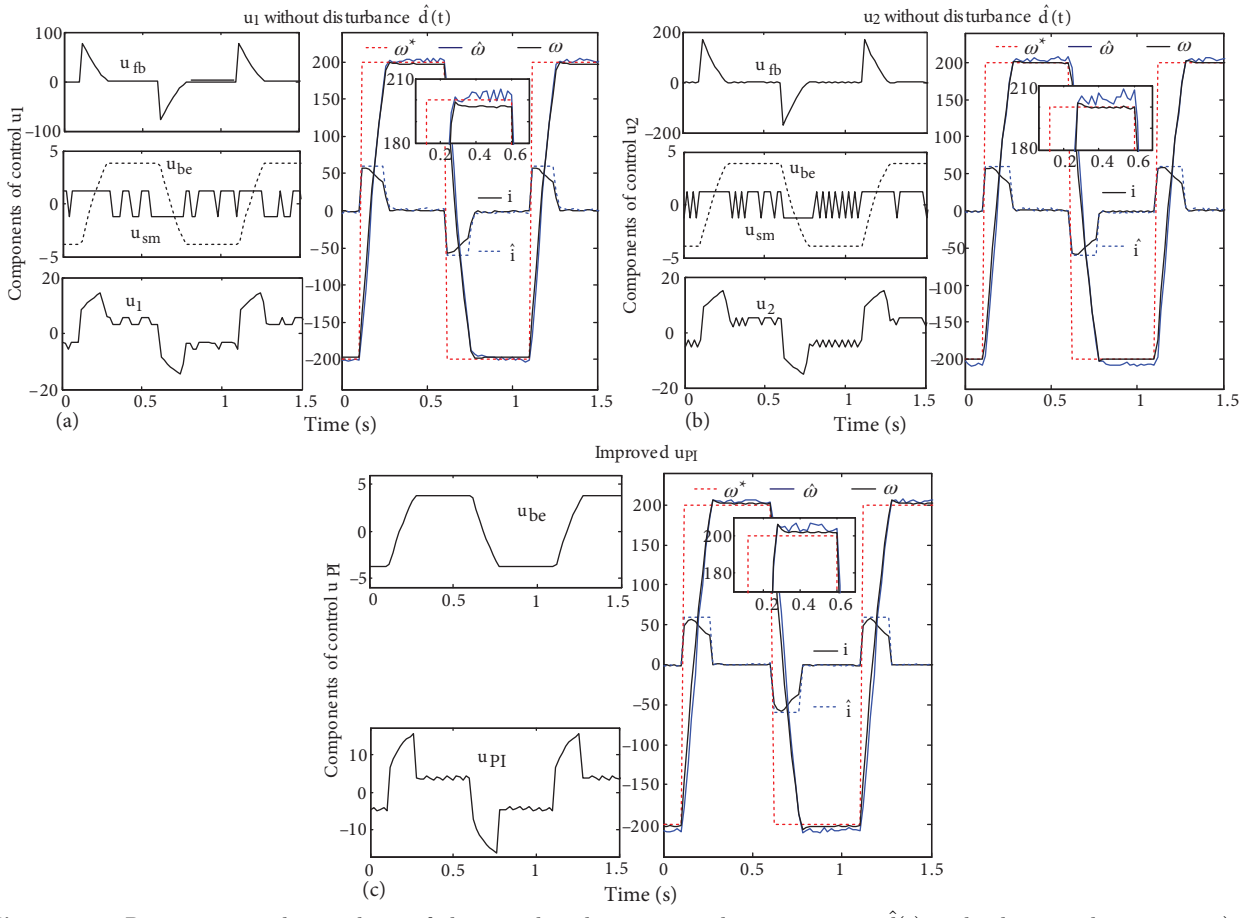

Figure 12. Responses in the tracking of the speed and current without injecting $\hat{d}(t)$ in both control versions: a) for u_1 and b) for u_2, respectively; c) response of the improved u_{PI}.

However, from simulation results, it is expected that the response of control version u_2 will be improved by injecting disturbance signal $\hat{d}(t)$. To verify this, control u_2 is examined by adding disturbance $\hat{d}(t)$, and the provided result is plotted in Figure 13a, where a better performance is obtained in the tracking of the current and the speed. In order to provide a better observation, a magnified response of the improved version u_{PI} and the proposed control versions u_1 and u_2 is plotted in Figure 13b, where it can be clearly seen that injecting $\hat{d}(t)$ into control u_2 improves the speed tracking at the transients and stabilizes the speed response in steady state, as well as improving the convergence of the speed estimation. Moreover, proposed control u_2 provides a slightly faster transient response in respect to other control versions u_1 and u_{PI}, which can be seen in Figure 13b.

The variation of the load inertia (by exchanging the flywheels) is reflected as external disturbances and/or mechanical parameter uncertainties in the drive system. Thus, the above results explore the controllers' robustness to uncertainties caused by load variations. Moreover, all 3 control versions are examined for various speed ranges in order to explore the controllers' robustness to a variation of the speed under load operation using the flywheel with J_1. First, the experiment is performed for a low-range reversal speed with 30 rad/s, and the obtained results are plotted in Figure 14. Comparing the results shown in Figures 14a–14c verifies that both of the proposed control versions, u_1 and u_2, exhibit better performance with respect to the improved u_{PI} in speed tracking. The current ripples are almost the same for all of the control versions. However, u_2 receives a higher current at the transient instants at this low range of speed and u_2 exhibits a faster transient response with respect to u_1 and the improved u_{PI}.

In addition, as done previously in Section 5, the speed tracking performance is also examined for varying stepped speed ranges (starting at 0 and increasing step-by-step to 50 rad/s, 100 rad/s, and 300 rad/s) and under a constant load (J_1) operation. The relevant results are plotted in Figure 15. In the sensorless drive, the improved u_{PI} control version provides a larger overshoot in current and speed (see Figure 15a) with respect to proposed control versions u_1 and u_2 (see Figures 15b and 15c), where u_2 exhibits a better speed tracking performance at 50 rad/s. In Figure 15, the currents are magnified at a multiplication of 10 for a better observation.

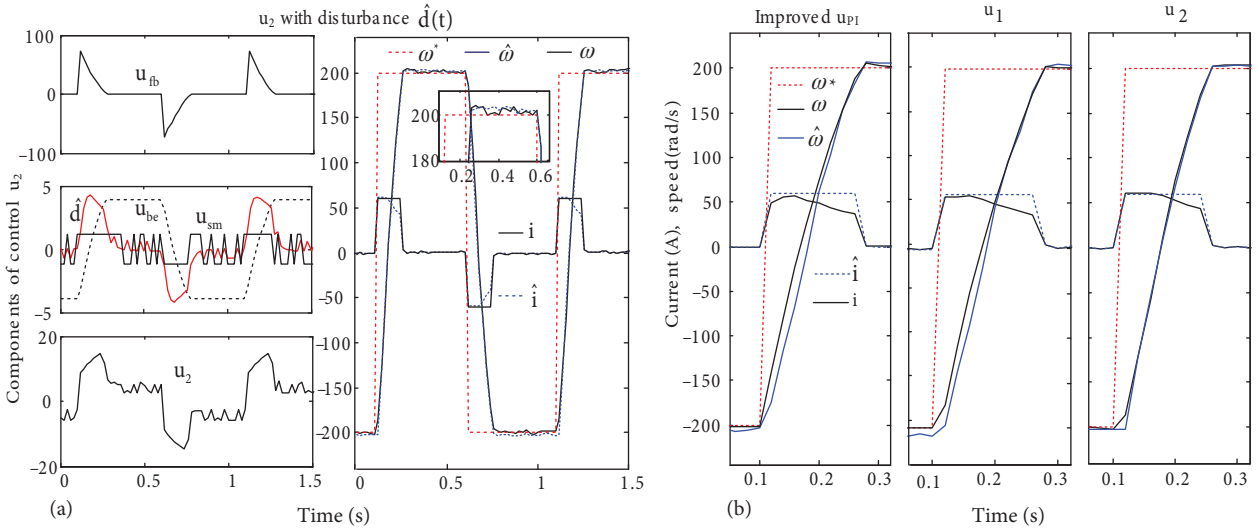

Figure 13. Response of the proposed control u_2: a) when disturbance signal is injected and b) a magnified performance comparison for control versions u_{PI}, u_1, and u_2, respectively.

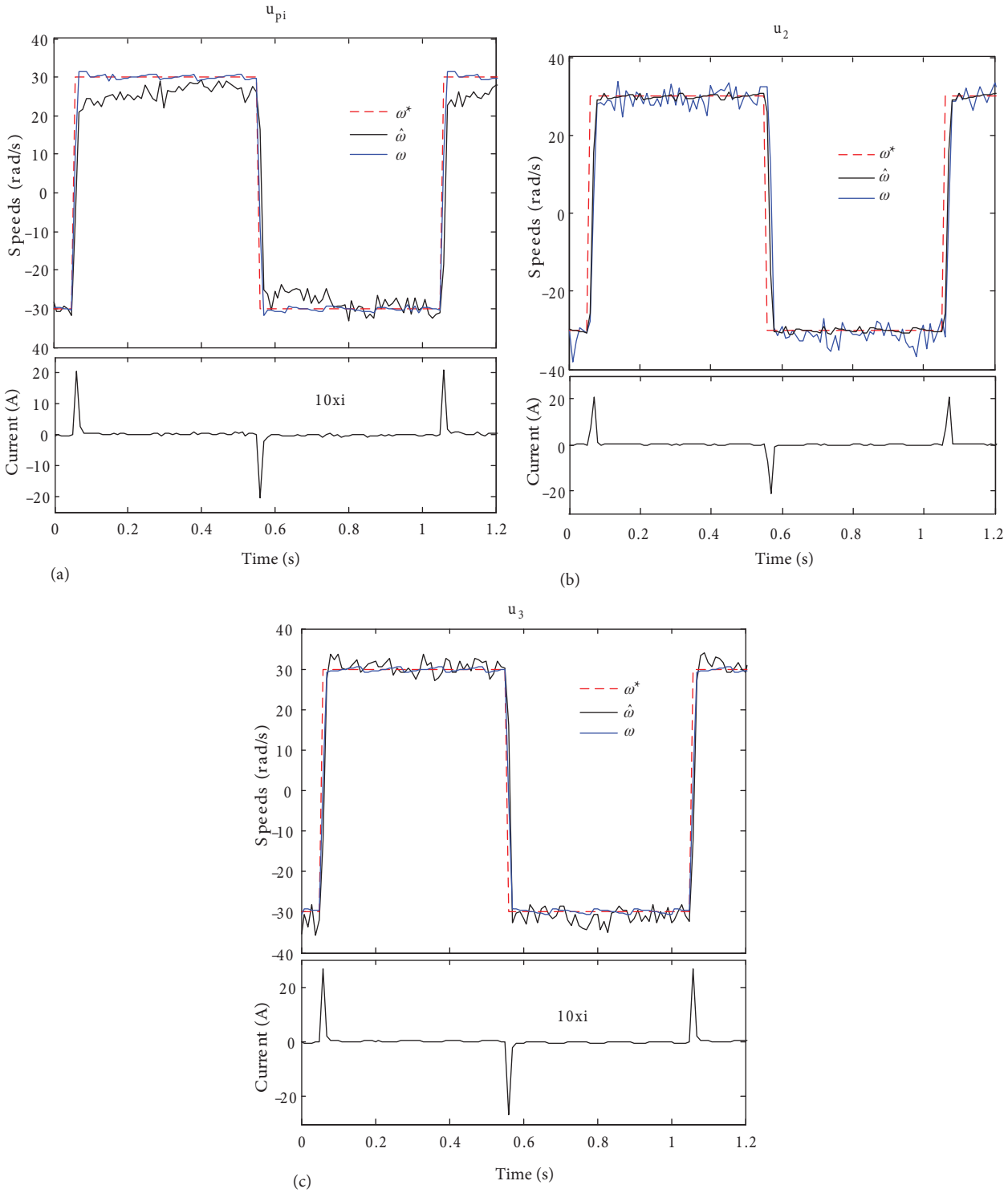

Figure 14. Experimental response of the control versions for a lower range reversal speed with 30 rad/s: a) for the improved u_{PI}, b) for u_1, and c) for u_2.

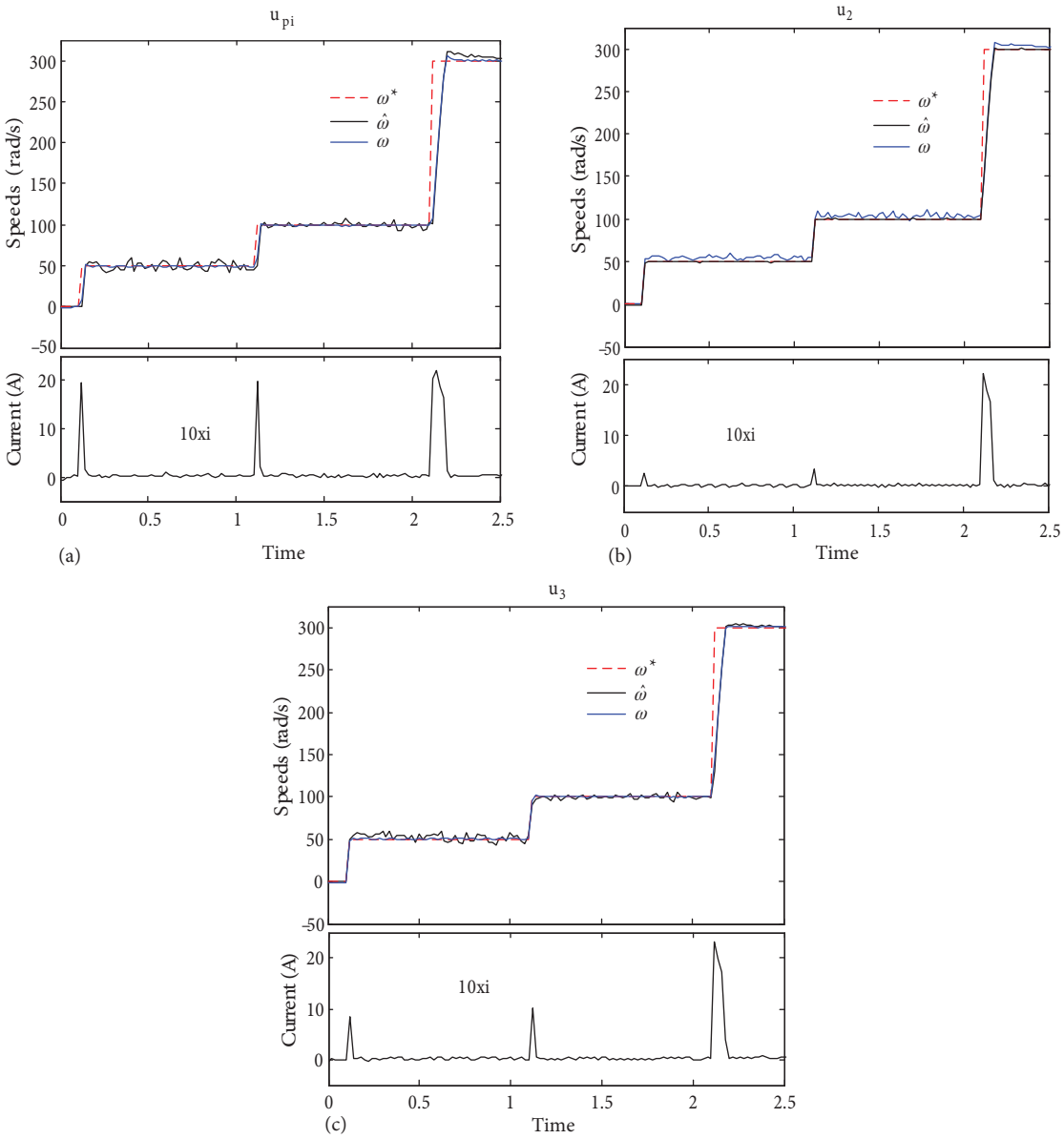

Figure 15. Experimental response of the control versions for several stepped speed ranges: a) for the improved u_{PI}, b) for u_1, and c) for u_2.

7. Conclusion

An enhancement to SMC with an interpretation of the equivalent control as the sum of the feedforward and proportional error feedback was validated by simulations and DSP-based experiments for a modified speed sensorless control of PM DC motor drives. The proposed control law was examined for 2 different sliding function variables, σ_1 and σ_2, and for 2 different load inertia, J_1 and J_2, as well as for different speed ranges.

- The use of the sliding function σ_2 and the adding of the proportional error feedback into the control, with injecting the feedforward component as well as reducing the discontinuous control gain, provide more stabilized tracking of the rotor speed and current, improving the convergence of the speed estimate, as well.

- Moreover, significant chattering suppression and current ripple reduction were achieved by proposed controls u_1 and u_2, without requiring a smoothing LPF. The reduction of the current ripple means the reduction of the torque pulsation in the motor drive control, which is a significant demand in industrial applications where a precise torque control is required and the load inertia varies from a very small value to a very large value (for example, paper machine winders). Thus, the proposed control version may be extended to large machine drives.

- Although the proposed SMC scheme uses a single-loop control structure and does not require any additional chattering reduction techniques or a LPF, it is very easy to regulate the rotor speed and current in a single loop, and the control performance is improved to some extent over that of the improved cascaded PI current/speed control scheme. However, in the combined single-loop controller, there is no mechanism to limit the rotor current, so it should be ensured that the rotor current is kept below the permitted maximum current rating during operation.

The unified sliding mode observer performance was also examined with respect to the variation of the load inertia, where the weakness of the observer occurs; thus, it necessitates that observer control gain L_1 be adapted to the load variation. Moreover, the convergence of the speed estimates fails at low speeds below 10 rad/s. This leads to the need for further study of the proposed control scheme improvement.

References

[1] Seborg DE, Edgar TF, Mellichamp DA. Process dynamics and control. New York, NY, USA: Wiley, 1989.

[2] Utkin VI. Variable structure systems with sliding modes. IEEE T Auto Contr 1977; 22: 212–222.

[3] DeCarlo RA, Zak SH, Matthews GP. Variable structure control of nonlinear multivariable systems: a tutorial. P IEEE 1988; 76: 212–232.

[4] Hung JY, Gao WB, Hung JC. Variable structure control: a survey. IEEE T Ind Electron 1993; 40: 1–22.

[5] Utkin VI. Sliding mode control design principles and applications to electric drives. IEEE T Ind Electron 1993; 40: 23–35.

[6] Sabanovic A, Jezernik K, Sabanovic N. Sliding modes applications in power electronics and electrical drives. In: Yu X, Xu JX, editors. Variable Structure Systems Towards the 21st Century. Berlin, Germany: Springer, 2002. pp. 223–251.

[7] Tan SC, Lai YM, Tse CK. General design issues of sliding-mode controllers in DC-DC converters. IEEE T Ind Electron 2008; 55: 1160–1173.

[8] Edwards C, Spurgeon SK. Sliding Mode Control: Theory and Applications. London, UK: Taylor & Francis, 1998.

[9] Halil HK. Nonlinear Systems. New Jersey, NJ, USA: Pearson, 2000.

[10] Utkin VI, Gulder J, Shi J. Sliding Mode Control in Electromechanical Systems. London, UK: Taylor & Francis, 1999.

[11] Lee H, Utkin VI. Chattering suppression methods in sliding mode control systems. Annu Rev Control 2007; 31: 179–188.

[12] Fridman L. An averaging approach to chattering. IEEE T Automat Contr 2001; 46: 1260–1265.

[13] Xu JX, Pan YJ, Lee TH. Sliding mode control with closed-loop filtering architecture for a class of nonlinear systems. IEEE T Circuits Syst 2004; 51: 168–173.

[14] Yu X, Kaynak O. Sliding-mode control with soft computing: a survey. IEEE T Ind Electron 2009; 56: 3275–3285.

[15] Ohnishi K, Matsui N, Hori Y. Estimation, identification, and sensorless control in motion control system. In: Bose BK, editor. Power Electronics and Variable Frequency Drives: Technology and Applications. Piscataway, NJ, USA: Wiley-IEEE Press, 1994. pp. 1253–1265.

[16] Hercog D, Curkovic M, Edilbehar G, Urlep E. Programming of the DSP-2 board with the MATLAB/Simulink. In: IEEE 2003 International Conference on Industrial Technology; 10–12 December 2003. Maribor, Slovenia: IEEE. pp. 709–713.

[17] Slotine JJE, Li W. Applied Nonlinear Control. Englewood Cliffs, NJ, USA: Prentice-Hall, 1991.

[18] Dal M. DSP based sensorless PM DC motor drives using a proportional plus sliding mode control. In: IFAC 2009 2nd Intelligent Conference of Control Systems and Signal Processing; 21–23 September 2009. İstanbul, Turkey: IFAC. pp. 1475–1479.

[19] Ohishi K, Nakao M, Ohnishi K. Microprocessor-controlled DC motor for load-insensitive position servo systems. IEEE T Ind Electron 1987; 34: 44–49.

[20] Chang FJ, Twu SH, Chang S. Tracking control of DC motors via an improved chattering alleviation control. IEEE T Ind Electron 1992; 39: 25–29.

[21] Buja GS, Menis R, Valla MI. Disturbance torque estimation in a sensorless DC Drive. IEEE T Ind Electron 1995; 42: 351–357.

[22] Pisano A, Davila A, Fridman L, Usai E. Cascade control of PM DC drives via second- order sliding-mode technique. IEEE T Ind Electron 2008; 55: 3846–3854.

[23] Dal M, Teodorescu R. Sliding mode controller gain adaptation and chattering reduction techniques for DSP based PM DC motor drives. Turk J Electr Eng Co 2011; 19: pp. 531–549.